Underlay D2D Communication in a Finite Cellular Network with Exclusion Zone

Jing Guo*, Salman Durrani*, Xiangyun Zhou*, and Halim Yanikomeroglu†
*Research School of Engineering, The Australian National University, Canberra, ACT 2601, Australia.
Emails: {jing.guo, salman.durrani, xiangyun.zhou}@anu.edu.au.
†Department of Systems and Computer Engineering, Carleton University, Ottawa, ON K1S 5B6, Canada.
Email: halim@sce.carleton.ca.

***Abstract*— In this paper, we consider underlay in-band device-to-device (D2D) communication in a finite cellular network region. To minimize the D2D interference generated at the base station (BS), we adopt the exclusion zone mechanism, i.e., only D2D users outside the BS exclusion zone share the same resource with the cellular uplink user. Using the stochastic geometry, we develop a general framework to analytically compute the outage probability at the center-located BS and the outage probability at an arbitrarily located D2D receiver in a disk-shaped network region. To quantify the overall D2D communication performance in the finite region, the average number of successful D2D transmissions is also derived. It shows that the D2D receiver close to the cell edge or the exclusion zone experiences lower outage probability compared to the D2D receiver not close to the edge region, which illustrates the location-dependent performance. Moreover, given the outage probability constraint at the BS, which is controlled by varying the radius of the exclusion zone, we find that there is an optimum D2D receiver sensitivity that results in the maximum average number of successful D2D transmissions. The results highlight the importance of carefully choosing system parameters to extract the benefit from the exclusion zone.**

I. Introduction

Device-to-device (D2D) communication is a promising technology for fifth generation (5G) wireless networks [1]. In D2D communication, nearby users can directly talk to each other without traversing through the base station (BS). This reduces the traffic burden at the BS and also improves the throughput and delay. In this work, we focus on the in-band underlay D2D communication, where D2D users share the same spectrum resource with cellular users. While such concurrent spectrum sharing improves the spectrum efficiency, it results in interference between D2D and cellular users. Thus, the interference management and modeling in in-band underlay D2D communication are important research problems.

For the D2D-enabled cellular network, the inter-cell interference can be managed very well by the inter-cell interference coordination (ICIC) mechanism, which is a widely adopted assumption in the literature [2–5]. In terms of the intra-cell interference, different interference management methods have been proposed in the literature. As identified in [6], the main approaches can be categorized into: i) mode selection, where users can switch across different modes (i.e., underlay D2D mode, cellular mode, etc.) according to certain criteria [2, 5, 7, 8]; ii) interference aware resource scheduling, where the available resources are scheduled among D2D users via different techniques (i.e., non-linear programming, game theory, etc.) [9–11]; and iii) other interference management techniques, such as power control, beamforming, and so on [3, 4, 12, 13]. Note that some of these techniques may involve higher computational overhead or require the channel information exchange which brings in the signaling overhead [6].

In this work, motivated by the principle of exclusion zone around the primary users in cognitive networks [14], we adopt a simple, distributed interference management technique to control the D2D intra-cell interference at the BS, i.e., no D2D transmission is allowed in the exclusion zone around the BS. To evaluate the impact of exclusion zone, the intra-cell interference modeling and characterization are crucial. Stochastic geometry is a powerful mathematical tool that allows the computation of tractable expressions and also encompasses the randomness of users [15]. Recently, some papers have analyzed the interference performance in D2D communication with exclusion zone [12, 13]. For analytical tractability, these works assumed the network region to be infinite and consequently the interference experienced at all the D2D users is the same.

In practice, the cellular network region is finite and the consideration of finite region allows us to capture the location-dependent performance of D2D users. However, it also poses complex technical challenges [16], since, under the exclusion zone mechanism, the distance correlation is caused by the locations of the BS, the typical D2D user and interfering users.

In this paper, we analyze the performance of underlay D2D communication in a disk-shape cellular network region with exclusion zone to manage the interference. Compared to previous works, the major contributions of this paper are:

- Using stochastic geometry, we derive the analytical expressions for the outage probability at the BS, and the outage probability at an arbitrarily located D2D receiver, under the scenario where the path-loss exponent on the cellular/interfering link is 2 or 4, and the fading on the desired D2D link is Nakagami-m fading. Our analytical expressions allow for fast computation of numerical results, avoiding the need for the time consuming simulation. It also illustrate the location-dependence performance for

This work was supported by the Australian Research Council's Discovery Project Funding Scheme (Project number DP170100939).

978-1-5090-5935-5/17/$31.00 ©2017 IEEE

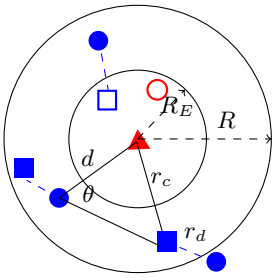

Fig. 1. Illustration of the network model (▲ = BS, ○ = CUE, ■ = DUE (p-DUE in underlay D2D mode), □ = p-DUE in silent mode, ● = DRx. Note that p-DUE and its corresponding DRx are connected by a dashed line).

D2D users, which cannot be characterized by the infinite network region assumption.

- To investigate the overall D2D communication performance, we consider the average number of successful D2D transmissions, which relies on the outage probability at the D2D receiver and the probability of being in D2D mode, as the performance metric. This derived result, together with the derived outage probability at the BS, are used to quantify the impact of exclusion zone.
- Based on our derived analytical results, we investigate the effect of D2D user's receiver sensitivity (i.e., the minimum required received power at the receiver due to the power control), given the outage constraint at the BS, which is controlled by the considered exclusion zone scheme. Our results show that there is an optimum receiver sensitivity that results in the maximum average number of successful D2D transmissions.

II. System Model

We consider a single cellular uplink network model for D2D communication, where the network region $\mathcal{A}$ is assumed to be a disk with radius R and the base station is located at the origin. All the users and BS are assumed to be equipped with omnidirectional antenna. We do not consider inter-cell interference in this work and it is assumed to be effectively dealt with using ICIC [2]. Hence, we only focus on the intra-cell interference between users. We consider that the uplink cellular users are scheduled to access the spectrum resource in a round-robin fashion and only one cellular user (CUE) is transmitting at any time. For analytical tractability, the location of the transmitting CUE is modeled as a uniform distribution in $\mathcal{A}$ [8]. Let z denote both the location and the CUE itself. Then the distribution of the distance between the BS and the CUE r_z is $f_{r_z}(r_z) = \frac{2r_z}{R^2}$. The network model is illustrated in Fig. 1.

D2D assumptions: There are multiple potential D2D users (p-DUEs) residing in region $\mathcal{A}$ and they intend to use the available uplink resource to implement the D2D communication, i.e., directly transmit to their desired D2D receivers (DRxs). The location of p-DUEs is modeled as a Poisson Point Process (PPP), denoted as Φ, with constant density λ in $\mathcal{A}$. For each p-DUE, its desired DRx is assumed to be uniformly distributed in the disk region centered at the p-DUE with radius R_D. According to the displacement theorem [15], the location of DRx is following an inhomogeneous PPP, denoted as Φ^{DRx}, with density λ^{DRx} in region $\mathcal{A}^{\text{DRx}}$, where $|\mathcal{A}^{\text{DRx}}| = \pi(R+R_D)^2$.[2] Note that the exact formulation of λ^{DRx} will be presented in Section IV-D. Let x_k denote both the k-th p-DUE and its location, and y_k denote the k-th DRx and its location, respectively. The distance distribution between the any p-DUE and DRX pair is $f_{R_d}(r_d) = \frac{2r_d}{R_D^2}$.

Exclusion zone: To reduce the interference at the BS, we employ the exclusion zone mechanism in this work. Specifically, there is an exclusion zone with radius R_{E} formed around the BS and no co-channel D2D transmissions are permitted in this region [13]. Only p-DUEs not inside this exclusion zone are allowed to operate in underlay D2D mode, i.e., share the same uplink resource with the CUE. These potential D2D users are known as DUEs.

Channel assumptions: We model the communication channel as the path-loss plus block fading channel model, i.e., the instantaneous received power at a receiver from a transmitter is $p_t g r^{-\alpha}$, where p_t is the transmit power, g is the fading power gain, r is the distance between the transmitter and receiver and α is the path-loss exponent. The desired link between a DUE and its desired DRx is more likely to be line-of-sight link as the D2D communication generally happens within a short range [7]. The path-loss exponent on this link is denoted as α_{L} and the fading on this link is assumed to be independently and identically distributed (i.i.d.) Nakagami-m fading. For the CUE-BS link and the interfering links on DUE-BS, DUE-DRx and CUE-DRx, they are likely to be non-line-of-sight links, where α_{N} represents the path-loss exponent and the fading on these links are assumed to be i.i.d. Rayleigh fading [7]. We assume $\alpha_{\text{L}} \leq \alpha_{\text{N}}$. The full channel inversion power control is also adopted in this work for uplink communication. Then the transmit powers for CUE and DUE are $\rho_c r_z^{\alpha_{\text{N}}}$ and $\rho_d r_d^{\alpha_{\text{L}}}$, respectively, where ρ_c and ρ_d are the BS' receiver sensitivity and DRx's receiver sensitivity, respectively.

Aggregate interference: Based on the above system model, the instantaneous aggregate interference at the BS and a typical DRx y_j are

$$I_{\text{agg}}^{\text{BS}} = \sum_{x_k \in \Phi} g_k^{\text{BS}} \rho_d r_{d_k}^{\alpha_{\text{L}}} r_{c_k}^{-\alpha_{\text{N}}} \mathbf{1}(r_{d_k} > R_{\text{E}}) \,, \tag{1a}$$

$$I_{\text{agg}}^{\text{DRx}}(x_j, y_j) = \frac{g_z \rho_c r_z^{\alpha_{\text{N}}}}{|z - y_j|^{\alpha_{\text{N}}}} + \sum_{x_k \in \Phi, k \neq j} \frac{g_k^{\text{DRx}} \rho_d r_{d_k}^{\alpha_{\text{L}}}}{|x_k - y_j|^{\alpha_{\text{N}}}} \mathbf{1}(r_{d_k} > R_{\text{E}}) \,, \tag{1b}$$

respectively, where $|z - y_j|$ is the Euclidean distance between the CUE and the typical DRx, $|x_k - y_j|$ is the Euclidean distance between the k-th p-DUE and the typical DRx, and $\mathbf{1}(\cdot)$ is the indicator function which models the exclusion zone mechanism.

[2] A more realistic model is that the DRxs are also residing in $\mathcal{A}$. In that way, when the p-DUE gets close to the cell-edge, the possible location of its DRx is no longer in a disk centered at the p-DUE and is bounded by the ragion $\mathcal{A}$. For analytical tractability, we adopt our presented model, i.e., the DRx is uniformly distributed in a disk region centered at the p-DUE, irrespective of the location of p-DUE. The numerical results from our presented model match very tightly with the simulation results from the more realistic model.

III. Performance Metrics

In this section, we present the performance metrics to evaluate the network performance. The metrics considered are the outage probability at the BS and an arbitrarily located DRx, and the average number of successful D2D transmissions.

Outage probability: For an interference-limited scenario, the outage probability, in general, is defined as the probability that the signal-to-interference ratio (SIR) at the receiver falls below a given threshold γ.

For the CUE-BS link, the outage probability at the BS is

$$P_{\text{out}}^{\text{BS}}(\gamma) = \mathbb{E}_{I_{\text{agg}}^{\text{BS}}, g_0^{\text{BS}}}\left\{ \Pr\left(\frac{g_0^{\text{BS}} \rho_c}{I_{\text{agg}}^{\text{BS}}} < \gamma \right) \right\} = 1 - \mathcal{M}_{I_{\text{agg}}^{\text{BS}}}(s)\Big|_{s=\frac{\gamma}{\rho_c}}, \tag{2}$$

where $\mathbb{E}\{\cdot\}$ is the expectation operator, $\mathcal{M}_{I_{\text{agg}}^{\text{BS}}}(s) = \mathbb{E}_{I_{\text{agg}}^{\text{BS}}}\left\{\exp\left(-sI_{\text{agg}}^{\text{BS}}\right)\right\}$ denotes the moment generating function (MGF) of $I_{\text{agg}}^{\text{BS}}$. The second step comes from the fact that the fading power gain on the CUE-BS link, g_0^{BS}, follows the exponential distribution.

As for the DRx, we assume that the typical DRx is located at the distance d away from the BS. Due to the symmetry of the network region, the outage probability at any DRx which is d away from the BS will be the same. By leveraging the fading on the desired DUE-DRx link being Nakagami-m fading, where m is assumed to be integer, we have the outage probability at the typical DRx as [5]

$$P_{\text{out}}^{\text{DRx}}(\gamma, d) = 1 - \sum_{t=0}^{m-1} \frac{(-s)^t}{t!} \frac{d^t}{ds^t} \mathcal{M}_{I_{\text{agg}}^{\text{DRx}}}(s, d)\Big|_{s=m\frac{\gamma}{\rho_d}}, \tag{3}$$

where $\mathcal{M}_{I_{\text{agg}}^{\text{DRx}}}(s, d)$ is the MGF of $I_{\text{agg}}^{\text{DRx}}$ experienced at the typical DRx.

Average number of successful D2D transmissions: The outage probability at a DRx only reflects the DUE's individual performance. There are multiple p-DUEs in region $\mathcal{A}$. Hence, we consider the metric, average number of successful D2D transmissions, to quantify the overall performance of underlay D2D communication. As the name suggests, it is the average number of underlay D2D users that can transmit successfully over the network region. According to [5], using the PPP assumption and the network symmetry, we can have its formulation given by

$$\bar{M} = \int_0^{R+R_D} \left(1 - P_{\text{out}}^{\text{DRx}}(\gamma, d)\right) p_{\text{D2D}}(d) \lambda^{\text{DRx}}(d) 2\pi d \, \mathrm{d}d, \tag{4}$$

where $p_{\text{D2D}}(d)$ is the probability of p-DUE being in D2D mode given its corresponding DRx's distance to BS is d, $\lambda^{\text{DRx}}(d)$ is the node density of DRxs, and $P_{\text{out}}^{\text{DRx}}(\gamma, d)$ is outage probability at the corresponding DRx. Note that $P_{\text{out}}^{\text{DRx}}(\gamma, d)$, $p_{\text{D2D}}(d)$ and $\lambda^{\text{DRx}}(d)$ are functions of distance d. Hence, (4) is able to incorporate the effect of guard zone and the boundary.

From (2), (3) and (4), in order to characterize the network performance, we need to obtain the MGF of the aggregate interference at the receiver ($\mathcal{M}_{I_{\text{agg}}^{\text{BS}}}(s)$ and $\mathcal{M}_{I_{\text{agg}}^{\text{DRx}}}(s, d)$), the probability of being in D2D mode $p_{\text{D2D}}(d)$, and the density function of DRx $\lambda^{\text{DRx}}(d)$. These results are presented in the next section.

IV. Performance Analysis

In this section, we present the analytical results needed to determine the network performance metrics.

A. MGF of the aggregate interference at the BS

Let I_k^{BS} denote the interference from k-th p-DUE to the BS. Because of the independent and uniformly distributed (i.u.d.) property of p-DUEs and i.i.d. property of fading channel, I_k^{BS} is also i.i.d.. Hence, we drop the index k in r_{c_k}, r_{d_k}, g_k, h_k and I_k^{BS}. The aggregate interference can then be written as $\left(I^{\text{BS}}\right)^M$, where M is the number of p-DUEs in $\mathcal{A}$ and it follows the Poisson distribution with density $\lambda|\mathcal{A}|$.

From the MGF's definition, the MGF of $I_{\text{agg}}^{\text{BS}}$ is

$$\begin{aligned}\mathcal{M}_{I_{\text{agg}}^{\text{BS}}}(s) =& \mathbb{E}_M\left[\mathbb{E}_{I^{\text{BS}}}\left[\exp\left(-s\left(I^{\text{BS}}\right)^M\right)\Big| M\right]\right] \\ =& \exp\Big(\lambda|\mathcal{A}|\big(\mathcal{M}_{I^{\text{BS}}}(s) - 1\big)\Big),\end{aligned} \tag{5}$$

where $\mathcal{M}_{I^{\text{BS}}}(s)$ denotes the MGF of the interference from an individual p-DUE. From (1a), only the p-DUEs outside the exclusion zone will generate interference. Thus, the MGF of I^{BS} is given by

$$\begin{aligned}\mathcal{M}_{I^{\text{BS}}}(s) =& \int_0^{R_D}\int_0^{\infty}\Bigg(\int_0^{R_{\text{E}}} \exp(-s\times 0)\, f_{R_c}(r_c)\mathrm{d}r_c \\ &+\int_{R_{\text{E}}}^{R} \exp\left(-sg\rho_d r_d^{\alpha_{\text{L}}} r_c^{-\alpha_{\text{N}}}\right) f_{R_c}(r_c)\mathrm{d}r_c\Bigg) f_G(g) f_{R_d}(r_d)\mathrm{d}g\mathrm{d}r_d \\ =& \frac{R_{\text{E}}^2}{R^2} + \int_0^{R_D}\int_{R_{\text{E}}}^{R}\left(1 - \frac{s\rho_d r_d^{\alpha_{\text{L}}}}{s\rho_d r_d^{\alpha_{\text{L}}} + r_c^{\alpha_{\text{N}}}}\right)\frac{2r_c}{R^2}\frac{2r_d}{R_D^2}\mathrm{d}r_c\mathrm{d}r_d \\ =& 1 - \Big[\Upsilon(x, R) - \Upsilon(x, R_{\text{E}})\Big]\Big|_0^{R_D},\end{aligned} \tag{6}$$

where

$$\Upsilon(p,q) = \begin{cases} \frac{\left({}_2F_1\left[1, \frac{2}{\alpha_{\text{N}}}; \frac{2+\alpha_{\text{N}}}{\alpha_{\text{N}}}; \frac{-q^{\alpha_{\text{N}}}}{s\rho_d p^{\alpha_{\text{L}}}}\right]\alpha_{\text{N}} + {}_2F_1\left[1, \frac{-2}{\alpha_{\text{N}}}; \frac{\alpha_{\text{L}}-2}{\alpha_{\text{N}}}; \frac{-q^{\alpha_{\text{N}}}}{s\rho_d p^{\alpha_{\text{L}}}}\right]\alpha_{\text{L}}\right)}{(p^2q^2)^{-1}R_D^2 R^2(\alpha_{\text{N}}+\alpha_{\text{L}})}, \\ \qquad\qquad\qquad\qquad\qquad\qquad\qquad\qquad\qquad\qquad \alpha_{\text{L}} \neq 2; \\ \frac{\text{G}\left[\left\{\left\{0, \frac{\alpha_{\text{N}}-2}{\alpha_{\text{N}}}\right\}, \{2\}\right\}, \left\{\{0,1\}, \left\{\frac{-2}{\alpha_{\text{N}}}\right\}\right\}, \frac{q^{\alpha_{\text{N}}}}{s\rho_d p^2}\right]}{(2p^2q^2)^{-1}R_D^2 R^2}, \quad \alpha_{\text{L}} = 2; \end{cases}$$

and given $f(x)$ is a function of x, the notation $[f(x)]\,|_a^b$ denotes $f(b) - f(a)$, $G[\{\cdot\}, \cdot]$ is the Meijer G-function, ${}_2F_1[\cdot, \cdot; \cdot; \cdot]$ denotes the ordinary hypergeometric function, and the final result in (6) is obtained using Mathematica.

B. MGF of the aggregate interference at the typical DRx

The derivation of the MGF of I^{DRx} is much more complicated since the interference experienced at the DRx is location-dependent. At first, we condition on a DRx y', which is d away from the BS. According to the Slivnyak's theorem, conditioning on a node at a certain location for a PPP does not change the distribution of the remaining point process [15]. Thus, similar to the derivation of (5), we have

$$\mathcal{M}_{I_{\text{agg}}^{\text{DRx}}}(s, d) = \exp\Big(\lambda(|\mathcal{A}|)\big(\mathcal{M}_{I^{\text{DRx}}}(s,d) - 1\big)\Big)\mathcal{M}_{I_C^{\text{DRx}}}(s,d), \tag{7}$$

where $\mathcal{M}_{I^{\text{DRx}}}(s,d)$ is the MGF of the interference from a p-DUE and $\mathcal{M}_{I_C^{\text{DRx}}}(s,d)$ is the MGF of the interference from the CUE. The main results are presented in the following two propositions.

Proposition 1: According to the system model in Section II, where the *exclusion zone* is implemented, under the path-loss exponent $\alpha_{\text{N}}=4$, the MGF of the interference from an i.u.d. p-DUE received at a DRx, which is distance d away from the BS, is

$$\mathcal{M}_{I^{\text{DRx}}}(s,d)=1-\int_0^{R_D}\frac{\sqrt{s\rho_D}r_d^{\frac{\alpha_{\text{L}}}{2}}}{R^2}\frac{2r_d}{R_D^2} \times \text{Im}\left\{\ln\frac{\beta_1\left(r_d^{\frac{\alpha_{\text{L}}}{2}},-\mathbf{i}\sqrt{s\rho_d},R^2-d^2,-4\mathbf{i}\sqrt{s\rho_d}d^2\right)}{\beta_1\left(r_d^{\frac{\alpha_{\text{L}}}{2}},-\mathbf{i}\sqrt{s\rho_d},R_{\text{E}}^2-d^2,-4\mathbf{i}\sqrt{s\rho_d}d^2\right)}\right\}\text{d}r_d, \tag{8}$$

where $\mathbf{i}$ is the complex operator, $\text{Im}\{\cdot\}$ is the imaginary part, $\beta_1(x,a,b,c)=ax+b+\sqrt{(ax+b)^2+cx}$. For the special case where $\alpha_{\text{L}}=2,\alpha_{\text{N}}=4$, $\alpha_{\text{L}}=\alpha_{\text{N}}=4$ and $\alpha_{\text{L}}=\alpha_{\text{N}}=2$, we can have the MGF in closed-form as shown in (9), (10) and (11) at the top of this page, where $\Psi_1(\cdot,\cdot,\cdot,\cdot)$ and $\Psi_2(\cdot,\cdot,\cdot,\cdot)$ are given in (21) and (22), respectively.

Proof: See Appendix A.

Proposition 2: According to the system model in Section II, under the path-loss exponent $\alpha_{\text{N}}=4$ or 2, the MGF of the interference from the CUE received at a DRx, which is distance d away from the BS, is

$$\mathcal{M}_{I_C^{\text{DRx}}}(s,d)=1 - \begin{cases}\text{Im}\left\{\frac{\left[\beta_2\left(x^2,1-\mathbf{i}\sqrt{s\rho_c},-d^2\frac{1+\mathbf{i}\sqrt{s\rho_c}}{1-\mathbf{i}\sqrt{s\rho_c}},\frac{-4\mathbf{i}d^4\sqrt{s\rho_c}}{(1-\mathbf{i}\sqrt{s\rho_c})^2}\right)\right]_0^R}{(\sqrt{s\rho_c})^{-1}R^2(1-\mathbf{i}\sqrt{s\rho_c})^2}\right\}, & \alpha_{\text{N}}=4;\\ \frac{\left[\beta_2\left(x^2,(s\rho_c+1)^2,d^2(s\rho_c-1),4d^4s\rho_c\right)\right]_0^R}{(s\rho_c)^{-1}R^2(s\rho_c+1)^3}, & \alpha_{\text{N}}=2;\end{cases} \tag{12}$$

where $\beta_2(x,a,b,c)=\sqrt{(ax+b)^2+c}-b\ln\left(ax+b+\sqrt{(ax+b)^2+c}\right)$.

Proof: The interference from the CUE to the typical DRx is $I_C^{\text{DRx}}=g\rho_c r_z^{\alpha_{\text{N}}}\left(r_z^2+d^2-2r_z d\cos\theta\right)^{\frac{-\alpha_{\text{N}}}{2}}$. Note there is no constraint on the CUE. Similar to (19), we have

$$\mathcal{M}_{I_C^{\text{DRx}}}(s,d)=1-\mathbb{E}_{r_z}\left\{\int_0^{\pi}\frac{s\rho_c r_z^{\alpha_{\text{N}}}}{s\rho_c r_z^{\alpha_{\text{N}}}+\left(r_z^2+d^2-2r_z d\cos\theta\right)^{\frac{\alpha_{\text{N}}}{2}}}\frac{1}{\pi}\text{d}\theta\right\}. \tag{13}$$

Then following the similar derivation presented in Appendix A, we can obtain the closed-form results for $\alpha_{\text{N}}=4$ and 2. Due to the space constraint, we skip the derivation here.

C. Probability of being in D2D mode

As described in Section II, only those p-DUEs not in the exclusion zone are in D2D mode. Based on the assumption of disk-shape network region and i.u.d. DRxs, we obtain the probability of being in D2D mode as shown in the following proposition.

Proposition 3: According to the system model in Section II, where the *exclusion zone* is implemented, the probability that a p-DUE is in D2D mode, given that its DRx's distance to the BS is d, is given by

- when $R_{\text{E}}\le R-2R_D$,

$$p_d(d)=\begin{cases}\left(1-\frac{R_{\text{E}}^2}{R_D^2}\right)\mathbf{1}(R_{\text{E}}<R_D), & 0\le d<\textbf{abs}(R_{\text{E}}-R_D);\\ 1-\frac{\psi(d,R_D,R_{\text{E}})}{\pi R_D^2}, & \textbf{abs}(R_{\text{E}}-R_D)\le d<R_{\text{E}}+R_D;\\ 1, & d\ge R_{\text{E}}+R_D;\end{cases} \tag{14}$$

- when $R_{\text{E}}>R-2R_D$,

$$p_d(d)=\begin{cases}0, & 0\le d<R_{\text{E}}-R_D;\\ 1-\frac{\psi(d,R_D,R_{\text{E}})}{\pi R_D^2}, & R_{\text{E}}-R_D\le d<R-R_D;\\ 1-\frac{\psi(d,R_D,R_{\text{E}})}{\psi(d,R_D,R)}, & R-R_D\le d<R_{\text{E}}+R_D;\\ 1, & d\ge R_{\text{E}}+R_D;\end{cases} \tag{15}$$

where $\textbf{abs}(\cdot)$ is the absolute operator and $\psi(d,r_1,r_2)$ denotes the overlap region between two disk regions with radii r_1 and r_2, respectively, which are separated by distance d, i.e., [17]

$$\psi(d,r_1,r_2)=r_1^2\text{acos}\left(\frac{d^2+r_1^2-r_2^2}{2dr_1}\right)+r_2^2\text{acos}\left(\frac{d^2+r_2^2-r_1^2}{2dr_2}\right) - \frac{\sqrt{2r_2^2(r_1^2+d^2)-r_2^2-(r_1^2-d^2)^2}}{2}. \tag{16}$$

Proof: See Appendix B.

D. Density function of DRx

The density function of DRx has been derived in [5] and we present its result in the following lemma for sake of completeness.

Lemma 1: For a disk network region of radius R, assume there are multiple p-DUEs, where their location is modeled as a PPP with constant density λ. Each p-DUE has a desired DRx which is uniformly distributed in a disk region formed around the p-DUE with radius R_D. Then, the location of DRxs follows a PPP, with the density

$$\lambda^{\text{DRx}}(d)=\begin{cases}\lambda, & 0\le d<R-R_D;\\ \lambda\frac{\psi(d,R_D,R)}{\pi R_D^2}, & R-R_D\le d\le R+R_D;\end{cases} \tag{17}$$

where $\psi(\cdot,\cdot,\cdot)$ is given in (16).

E. Summary

Based on the above derivations, we can obtain: (i) *outage probability at the BS* by combining (6) with (5) and substituting into (2) (valid for any α_{N} and α_{L}); (ii) *outage probability at a DRx* by combining (7) with the results in Propositions 1 and 2 and substituting into (3) (valid for $\alpha_{\text{N}}=2$ and 4 with any α_{L}); and (iii) *average number of successful D2D transmissions* by substituting the outage probability at a DRx and results in Proposition 3 and Lemma 1 into (4).

$$\mathcal{M}_{I^{\mathrm{DRx}}}(s,d)=1-\begin{cases}\dfrac{\mathrm{Im}\left\{\left[\Psi_1\left(x,-\mathbf{i}\sqrt{s\rho_d},R^2-d^2,-4\mathbf{i}\sqrt{s\rho_d}d^2\right)-\Psi_1\left(x,-\mathbf{i}\sqrt{s\rho_d},R_{\mathrm{E}}^2-d^2,-4\mathbf{i}\sqrt{s\rho_d}d^2\right)\right]\right|_0^{R_D}\right\}}{(\sqrt{s\rho_d})^{-1}R_D^2R^2}, & \alpha_{\mathrm{L}}=2,\alpha_{\mathrm{N}}=4; \quad (9)\\ \dfrac{\mathrm{Im}\left\{\left[\Psi_2\left(x^2,-\mathbf{i}\sqrt{s\rho_d},R^2-d^2,-4\mathbf{i}\sqrt{s\rho_d}d^2\right)-\Psi_2\left(x^2,-\mathbf{i}\sqrt{s\rho_d},R_{\mathrm{E}}^2-d^2,-4\mathbf{i}\sqrt{s\rho_d}d^2\right)\right]\right|_0^{R_D}\right\}}{(\sqrt{s\rho_d})^{-1}R_D^2R^2}, & \alpha_{\mathrm{L}}=\alpha_{\mathrm{N}}=4; \quad (10)\\ \dfrac{\left[\Psi_2\left(x^2,s\rho_d,R^-d^2,4d^2s\rho_d\right)-\Psi_2\left(x^2,s\rho_d,R_{\mathrm{E}}^2-d^2,4d^2s\rho_d\right)\right]\big|_0^{R_D}}{(s\rho_d)^{-1}R_D^2R^2}, & \alpha_{\mathrm{L}}=\alpha_{\mathrm{N}}=2; \quad (11)\end{cases}$$

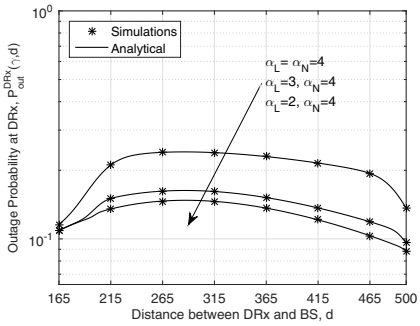

(a) Outage probability at the DRx.

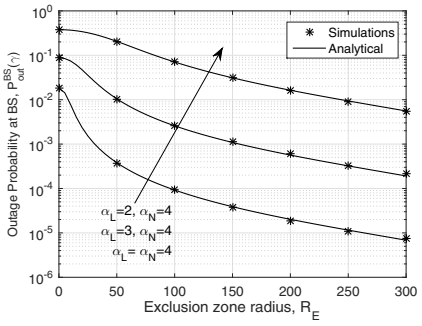

(b) Outage probability at the BS.

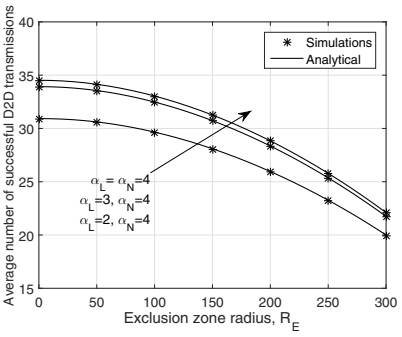

(c) Average number of successful D2D transmissions.

Fig. 2. System model validation.

V. Results

In this section, we present numerical and simulation results to investigate the network performance. The simulation results are generated based on the more realistic model described in footnote 1 (i.e., DRxs are confined in region $\mathcal{A}$), which is averaged over 10^6 Monte Carlo simulation runs. Unless specified otherwise, we set $R = 500$ m, $R_D = 35$ m, $\rho_c = -80$ dBm, $\rho_d = -70$ dBm, $\lambda = 5 * 10^{-5}$ users/m^2, SIR threshold $\gamma = 1$ and $m = 2$ for Nakagami-m fading on the desired D2D link.

A. Outage probability at the typical DRx

Fig. 2(a) plots the outage probability at the typical DRx versus its distance to the BS d with different path-loss exponent sets and $R_{\mathrm{E}} = 200$ m. It shows that our derived analytical results match exactly with the simulation results, which validates the accuracy of our analysis. According to Fig. 2(a), as the distance d increases, the outage probability at the typical DRx first increases and then decreases. This is greatly different from the infinite network system where the outage probability experienced at all the receivers is the same. *This highlights the importance of our analysis as the location-dependent performance cannot be captured by homogeneous PPP assumption.* Note that such location-dependent performance for DRxs is caused by the boundary effect. For the DRx close to the cell-boundary or exclusion zone, it will receive less interference compared with the DRx located in the middle, since the interfering DUEs are generally located on its one side only and not all around it.

B. Impact of exclusion zone radius

Figs. 2(b) and 2(c) plot the exclusion zone radius versus the outage probability at the BS and the average number of successful D2D transmissions with different path-loss exponent sets, respectively. Again, our analytical results provide a very good match with the simulation results.

These figures show that increasing the exclusion zone radius, on the one hand, improves the BS's performance; on the other hand, it reduces the average number of successful D2D transmissions. This is due to the fact that, as R_{E} increases, less number of p-DUEs are allowed to operate in D2D mode thereby reducing the interference at both BS and DRxs. The average number of successful D2D transmissions are determined by the number of DUEs and the outage probability at the DRx. Although the outage probability at DRx is improved with increasing R_{E}, the overall number of DUEs is reduced a lot especially when R_{E} is large. Hence, $\bar{M}$ decreases.

From Figs. 2(b) and 2(c), we can also see that, under $\alpha_{\mathrm{N}} = 4$, both $P_{\mathrm{out}}^{\mathrm{BS}}(\gamma)$ and $\bar{M}$ achieve the best performance for $\alpha_{\mathrm{L}} = 2$ and the worst performance for $\alpha_{\mathrm{L}} = 4$. This is caused by the adopted full channel inversion power control. A larger value of α_{L} implies the higher transmit power for DUEs, which introduces more interference and degrades the performance.

C. Effect of receiver sensitivity

From the previous subsection, we note that different values of exclusion zone radius result in different network performance. In order to study the effect of DRx's receiver sensitivity ρ_d in a fair manner, we adopt the following approach [5]: given $P_{\mathrm{out}}^{\mathrm{BS}}(\gamma) = 10^{-2}$, we can find the minimum value of R_{E} for each DRx's receiver sensitivity which satisfies the requirement; using this R_{E}, we then work out the average number of successful D2D transmissions.

Fig. 3 plots the receiver sensitivity of DRx versus the average number of successful D2D transmissions, for different p-DUE's density and path-loss exponent sets, under $P_{\mathrm{out}}^{\mathrm{BS}}(\gamma) = 10^{-2}$. *It shows that, as the receiver sensitivity*

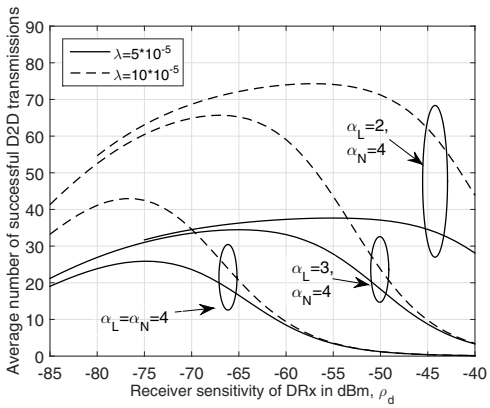

Fig. 3. DRx's receiver sensitivity ρ_d versus average number of successful D2D transmissions, with $P_{\text{out}}^{\text{BS}}(\gamma) = 10^{-2}$.

decreases, $\bar{M}$ first increases and then decreases. This can be explained as follows. The average number of successful D2D transmissions is impacted by both the number of DUEs and the outage probability at the DRx. With ρ_d decreasing, more p-DUEs can operate in underlay D2D mode since the individual generated interference is reduced. At first, the number of DUEs dominates the performance of $\bar{M}$ and the trend of $\bar{M}$ is increasing. Once ρ_d becomes very small, DRxs will receive the severe interference generated by the BS and a lot of DUEs. Hence, the outage probability at the DRx is adversely affected, which results in the loss of $\bar{M}$ that cannot be compensated by the large number of DUEs. Thus, the trend of $\bar{M}$ becomes decreasing later on. From the figure, we can also see that, for different transmission environments (i.e., different path-loss sets), the value of ρ_d achieving the maximum $\bar{M}$ varies. For example, a higher value of ρ_d is required for $\alpha_{\text{L}} = 2$ in order to achieve the maximum average number of successful D2D transmissions, compared to the case where $\alpha_{\text{L}} > 2$.

VI. Conclusions

In this paper, we have presented a mathematical framework to investigate the network performance in a D2D-enabled cellular network with the disk-shaped network region, where the exclusion zone mechanism is employed to manage the interference generated at the BS. By leveraging the stochastic geometry, we derived the outage probability at the BS, the outage probability at an arbitrarily located D2D receiver, and the average number of successful D2D transmissions which determines the overall performance of D2D communication. Our numerical results highlighted the location-dependent performance for D2D users and illustrated the impact of exclusion zone.

Appendix

A. Derivation of Proposition 1

Proof: According to our considered exclusion zone scheme, the interference from a p-DUE is

$$I^{\text{DRx}} = \begin{cases} g\rho_d r_d^{\alpha_{\text{L}}} \left(r_c^2 + d^2 - 2r_c d\cos\theta\right)^{\frac{-\alpha_{\text{N}}}{2}}, & R_{\text{E}} \le r_c \le R; \\ 0, & 0 \le r_c < R_{\text{E}}; \end{cases} \tag{18}$$

where $(r_c^2 + d^2 - 2r_c d\cos\theta)^{1/2}$ is the distance between the typical DRx and a p-DUE which is distance r_c from the BS, θ is the angle formed between the p-DUE-BS and DRx-BS which follows uniform distribution within 0 and 2π.

We then can express the MGF of I^{DRx} as

$$\begin{aligned} \mathcal{M}_{I^{\text{DRx}}}(s,d) =& \mathbb{E}_{r_d,\theta,g}\left\{\int_0^{R_{\text{E}}} \exp(-s\times 0)\, f_{R_c}(r_c)\mathrm{d}r_c \right. \\ &\left. + \int_{R_{\text{E}}}^{R} \exp\left(\frac{-s\rho_d r_d^{\alpha_{\text{L}}} g}{\left(r_c^2+d^2-2r_c d\cos\theta\right)^{\frac{\alpha_{\text{N}}}{2}}}\right) f_{R_c}(r_c)\mathrm{d}r_c\right\} \\ =& \frac{R_{\text{E}}^2}{R^2} + \mathbb{E}_{r_d,\theta}\left\{\int_{R_{\text{E}}}^{R}\left(\frac{\left(r_c^2+d^2-2r_c d\cos\theta\right)^{\frac{\alpha_{\text{N}}}{2}}}{s\rho_d r_d^{\alpha_{\text{L}}} + \left(r_c^2+d^2-2r_c d\cos\theta\right)^{\frac{\alpha_{\text{N}}}{2}}}\right)\frac{2r_c}{R^2}\mathrm{d}r_c\right\} \\ =& 1 - \mathbb{E}_{r_d}\left\{\int_{R_{\text{E}}}^{R}\int_0^{\pi} \frac{s\rho_d r_d^{\alpha_{\text{L}}}}{s\rho_d r_d^{\alpha_{\text{L}}} + \left(r_c^2+d^2-2r_c d\cos\theta\right)^{\frac{\alpha_{\text{N}}}{2}}}\frac{1}{\pi}\frac{2r_c}{R^2}\mathrm{d}\theta\mathrm{d}r_c\right\}. \end{aligned} \tag{19}$$

Because of the complicated form of integrand as shown in (19), we can only obtain a semi-closed form result with one-fold integral under $\alpha_{\text{N}} = 4$ and 2, and the closed-form results exist if $\alpha_{\text{L}} = 2$ or 4 is further assumed.

When $\alpha_{\text{N}} = 4$, the derivation is displayed in (20) at the top of next page, where $\beta_1(x,a,b,c) = ax+b+\sqrt{(ax+b)^2+cx}$, the second and third steps come from (2.553) and (2.261) in [18], respectively.

The closed-form results of (20) only exist for $\alpha_{\text{L}} = 2$ and 4. For $\alpha_{\text{L}} = 2$, using Mathematica, we get $\int_x 2x^2\beta_1(x,a,b,c)\mathrm{d}x = \Psi_1(x,a,b,c)$, where

$$\begin{aligned} \Psi_1(x,a,b,c) =& \frac{-x^2}{9} + \frac{2x^3}{3}\ln(\beta_1(x,a,b,c)) \\ &- \frac{\sqrt{(ax+b)^2+cx}}{72a^5\left(78abc+15c^2-32a^3bx+8a^4x^2+10a^2(8b^2-cx)\right)^{-1}} \\ &+ \frac{\ln\left(c+2a^2x+2a\left(b+\sqrt{(ax+b)^2+cx}\right)\right)}{48a^6(32a^3b^3+72a^2b^2c+36abc^2+5c^3)^{-1}}. \end{aligned} \tag{21}$$

For $\alpha_{\text{L}} = 4$, we set $r_d^2 = x$ and obtain $\int_x x\beta_1(x,a,b,c)\mathrm{d}x = \Psi_2(x,a,b,c)$, where

$$\begin{aligned} \Psi_2(x,a,b,c) =& \frac{-x^2}{8} + \frac{(10ab+3c-2a^2x)\sqrt{(ax+b)^2+cx}}{16} \\ &+ \frac{x^2}{2}\ln(\beta_1(x,a,b,c)) - \frac{\ln\left(c+2a^2x+2a\left(b+\sqrt{(ax+b)^2+cx}\right)\right)}{32a^4(16a^2b^2+16abc+3c^2)^{-1}}. \end{aligned} \tag{22}$$

Hence, we arrive the results in (9) and (10).

When $\alpha_{\text{N}} = 2$, since α_{L} is less or equal to α_{N} and the minimum value for the path-loss exponent is 2, we then can obtain the result for $\alpha_{\text{L}} = \alpha_{\text{N}} = 2$ following the similar derivation procedure for $\alpha_{\text{L}} = 4$. Due to the space limitation, we do not present the detailed derivation here. ■

B. Derivation of Proposition 3

Proof: Under the exclusion zone scheme, only the p-DUE outside the exclusion zone is in D2D mode. Instead of considering that there is a DRx uniformly distributed around the p-DUE, we consider that for each DRx, there is a p-DUE which is uniformly distributed inside the disk region formed

$$\mathcal{M}_{I^{\mathrm{DRx}}}(s,d)=1-\mathbb{E}_{r_d}\left\{\int_{R_{\mathrm{E}}}^{R}\int_0^{\pi}\frac{s\rho_D r_d^{\alpha_{\mathrm{L}}}}{2\mathbf{i}\sqrt{s\rho_D r_d^{\alpha_{\mathrm{L}}}}}\left(\frac{1}{r_c^2+d^2-2r_c d\cos\theta-\mathbf{i}\sqrt{s\rho_D r_d^{\alpha_{\mathrm{L}}}}}-\frac{1}{r_c^2+d^2-2r_c d\cos\theta+\mathbf{i}\sqrt{s\rho_D r_d^{\alpha_{\mathrm{L}}}}}\right)\frac{1}{\pi}\frac{2r_c}{R^2}\mathrm{d}\theta\mathrm{d}r_c\right\}$$

$$=1-\mathbb{E}_{r_d}\left\{\frac{\sqrt{s\rho_D r_d^{\alpha_{\mathrm{L}}}}}{2\mathbf{i}R^2}\int_{R_{\mathrm{E}}}^{R}\left(\frac{1}{\sqrt{(r_c^2+d^2-\mathbf{i}\sqrt{s\rho_D r_d^{\alpha_{\mathrm{L}}}})^2-4r_c^2d^2}}-\frac{1}{\sqrt{(r_c^2+d^2+\mathbf{i}\sqrt{s\rho_D r_d^{\alpha_{\mathrm{L}}}})^2-4r_c^2d^2}}\right)2r_c\,\mathrm{d}r_c\right\}$$

$$=1-\int_0^{R_D}\frac{\sqrt{s\rho_D}r_d^{\frac{\alpha_{\mathrm{L}}}{2}}}{R^2}\mathrm{Im}\left\{\ln\frac{\beta_1\left(r_d^{\frac{\alpha_{\mathrm{L}}}{2}},-\mathbf{i}\sqrt{s\rho_d},R^2-d^2,-4\mathbf{i}\sqrt{s\rho_d}d^2\right)}{\beta_1\left(r_d^{\frac{\alpha_{\mathrm{L}}}{2}},-\mathbf{i}\sqrt{s\rho_d},R_{\mathrm{E}}^2-d^2,-4\mathbf{i}\sqrt{s\rho_d}d^2\right)}\right\}\frac{2r_d}{R_D^2}\,\mathrm{d}r_d. \tag{20}$$

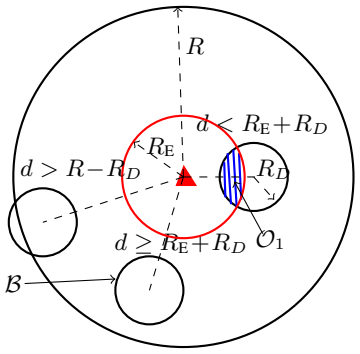

Fig. 4. Illustration of Proposition 3.

around it (denoted as $\mathcal{B}$). Note that when the DRx gets close to the cell edge, the possible location of p-DUE is the overlap region of $\mathcal{A}$ and $\mathcal{B}$.

Let us first consider the case where $R_D \leq R_{\mathrm{E}} \leq R-2R_D$. As shown in Fig 4, when $d < R_{\mathrm{E}}+R_D$, there is always an overlap region (denoted as $\mathcal{O}_1$) between the exclusion zone and the disk region πR_D^2 centered at the typical DRx. $\mathcal{O}_1 = \pi R_D^2$ if $d \subset [0, R_{\mathrm{E}}-R_D]$, and $\mathcal{O}_1 = \psi(d, R_D, R_{\mathrm{E}})$ if $d \subset [R_{\mathrm{E}}-R_D, R_{\mathrm{E}}+R_D]$, where $\psi(\cdot,\cdot,\cdot)$ is given in (16). When the p-DUE is inside the overlap region (i.e., the shaded region), it is not allowed to be in D2D mode since its distance to the BS is always less than R_{E}. As a result, the probability of being in D2D mode is $p_d(d) = 1-\frac{\mathcal{O}_1}{\pi R_D^2}$. Once $d > R_{\mathrm{E}}+R_D$, there is no overlap region such that $p_d(d)$ is always one.

Under the case where $R_{\mathrm{E}} \leq R_D$, $p_d(d)$ is the same as the previous case except for the range of $[0, R_{\mathrm{E}}-R_D]$. Within this range, $\mathcal{O}_1 = \pi R_{\mathrm{E}}^2$ but not πR_D^2.

As for the case of $R_{\mathrm{E}} > R-2R_D$, the possible location of p-DUE is no longer a disk region but the overlap region of $\mathcal{A}$ and $\mathcal{B}$ once $d > R-R_D$. Thus, for $d \subset [R-R_D, R_{\mathrm{E}}+R_D]$, $p_d(d)$ becomes $1-\frac{\mathcal{O}_1}{\psi(d,R_D,R)}$ but not $1-\frac{\mathcal{O}_1}{\pi R_D^2}$. The remaining part is the same as before. Hence, we arrive the result in Proposition 3. ■

REFERENCES

[1] J. Liu, N. Kato, J. Ma, and N. Kadowaki, "Device-to-device communication in LTE-Advanced networks: A survey," *IEEE Commun. Surveys Tuts.*, vol. 17, no. 4, pp. 1923–1940, Fourthquarter 2015.

[2] H. Min, W. Seo, J. Lee, S. Park, and D. Hong, "Reliability improvement using receive mode selection in the device-to-device uplink period underlaying cellular networks," *IEEE Trans. Wireless Commun.*, vol. 10, no. 2, pp. 413–418, Feb. 2011.

[3] N. Lee, X. Lin, J. Andrews, and R. Heath, "Power control for D2D underlaid cellular networks: Modeling, algorithms, and analysis," *IEEE J. Sel. Areas Commun.*, vol. 33, no. 1, pp. 1–13, Jan. 2015.

[4] M. Lin, J. Ouyang, and W. P. Zhu, "Joint beamforming and power control for device-to-device communications underlaying cellular networks," *IEEE J. Sel. Areas Commun.*, vol. 34, no. 1, pp. 138–150, Jan. 2016.

[5] J. Guo, S. Durrani, X. Zhou, and H. Yanikomeroglu, "Device-to-device communication underlaying a finite cellular network region," *IEEE Trans. Wireless Commun.*, vol. 16, no. 1, pp. 332–347, Jan. 2017.

[6] A. Asadi, Q. Wang, and V. Mancuso, "A survey on device-to-device communication in cellular networks," *IEEE Commun. Surveys Tuts.*, vol. 16, no. 4, pp. 1801–1819, Fourthquarter 2014.

[7] M. Peng, Y. Li, T. Q. S. Quek, and C. Wang, "Device-to-device underlaid cellular networks under Rician fading channels," *IEEE Trans. Wireless Commun.*, vol. 13, no. 8, pp. 4247–4259, Aug. 2014.

[8] X. Lin, J. G. Andrews, and A. Ghosh, "Spectrum sharing for device-to-device communication in cellular networks," *IEEE Trans. Wireless Commun.*, vol. 13, no. 12, pp. 6727–6740, Dec. 2014.

[9] C. Xu, L. Song, Z. Han, D. Li, and B. Jiao, "Resource allocation using a reverse iterative combinatorial auction for device-to-device underlay cellular networks," in *Proc. IEEE GLOBECOM*, Dec. 2012, pp. 4542–4547.

[10] W. Cheng, X. Zhang, and H. Zhang, "Optimal power allocation with statistical QoS provisioning for D2D and cellular communications over underlaying wireless networks," *IEEE J. Sel. Areas Commun.*, vol. 34, no. 1, pp. 151–162, Jan. 2016.

[11] Y. Xiao, K. C. Chen, C. Yuen, Z. Han, and L. A. DaSilva, "A Bayesian overlapping coalition formation game for device-to-device spectrum sharing in cellular networks," *IEEE Trans. Wireless Commun.*, vol. 14, no. 7, pp. 4034–4051, 2015.

[12] J. Ye and Y. J. Zhang, "A guard zone based scalable mode selection scheme in D2D underlaid cellular networks," in *Proc. IEEE ICC*, 2015, pp. 2110–2116.

[13] G. George, K. Ratheesh, and A. L. Mungara, "An analytical framework for device-to-device communication in cellular networks," *IEEE Trans. Wireless Commun.*, vol. 14, no. 11, pp. 6297–6310, Nov. 2015.

[14] J. Guo, S. Durrani, and X. Zhou, "Performance analysis of arbitrarily-shaped underlay cognitive networks: Effects of secondary user activity protocols," *IEEE Trans. Commun.*, vol. 63, no. 2, pp. 376–389, Feb. 2015.

[15] M. Haenggi, *Stochastic Geometry for Wireless Networks*. Cambridge University Press, 2012.

[16] J. Guo, S. Durrani, and X. Zhou, "Outage probability in arbitrarily-shaped finite wireless networks," *IEEE Trans. Commun.*, vol. 62, no. 2, pp. 699–712, Feb. 2014.

[17] E. W. Weisstein, "Circle-circle intersection," *MathWorld*. [Online]. Available: http://mathworld.wolfram.com/Circle-CircleIntersection.html

[18] I. S. Gradshteyn and I. M. Ryzhik, *Table of Integrals, Series, and Products*, 7th ed. Academic Press, 2007.